

Activity-Induced Collapse and Arrest of Active Polymer RingsEmanuele Locatelli^{1,*}, Valentino Bianco², and Paolo Malgaretti^{3,4,5}¹*Faculty of Physics, University of Vienna, Vienna 1090, Austria*²*Faculty of Chemistry, Chemical Physics Department, Complutense University of Madrid, Plaza de las Ciencias, Ciudad Universitaria, Madrid 28040, Spain*³*Max Planck Institute for Intelligent Systems, Heisenbergstrasse 3, 70569 Stuttgart, Germany*⁴*IV Institute for Theoretical Physics, University of Stuttgart, Pfaffenwaldring 57, 70569 Stuttgart, Germany*⁵*Helmholtz Institut Erlangen-Nürnberg for Renewable Energy (IEK-11), Forschungszentrum Jülich, Fürther Strasse 248, 90429 Nürnberg, Germany* (Received 20 July 2020; revised 24 January 2021; accepted 1 February 2021; published 1 March 2021)

We investigate, using numerical simulations, the conformations of isolated active ring polymers. We find that their behavior depends crucially on their size: Short rings ($N \lesssim 100$) swell, whereas longer rings ($N \gtrsim 200$) collapse, at sufficiently high activity. By investigating the nonequilibrium process leading to the steady state, we find a universal route driving both outcomes; we highlight the central role of steric interactions, at variance with linear chains, and of topology conservation. We further show that the collapsed rings are arrested by looking at different observables, all underlining the presence of an extremely long timescales at the steady state, associated with the internal dynamics of the collapsed section. Finally, we found that in some circumstances the collapsed state spins about its axis.

DOI: [10.1103/PhysRevLett.126.097801](https://doi.org/10.1103/PhysRevLett.126.097801)

Active matter systems, such as synthetic and biological swimmers, show remarkable single-particle and collective dynamics that are completely different from their equilibrium counterparts [1]. For example, their active motion leads single active particles to accumulate at walls [2,3] or at fluid interfaces [4,5] and to the onset of motility-induced phase separation (MIPS) for dense suspensions [6]. Up to now, the majority of the studies have focused on “simple” active systems that lack “internal” degrees of freedom, such as colloids. However, recent works on more complex active systems, like active polymers, have shown rich and counterintuitive dynamics [7–16]. For example, tangentially active polymers (i.e., polymers for which the active force acts tangentially to their backbone) undergo a coil-to-globule transition upon increasing the activity [13] and show a size-independent diffusion [13,14].

Such systems are far from being a purely theoretical speculation. Chains of active colloids can be assembled using state-of-the-art synthesis techniques [10]; furthermore, experiments with living worms (regarded as tangentially active polymers) have shown the onset of phase separation [17] akin to active colloids. Moreover, biological filaments such as DNA, RNA, actin, and microtubules experience the force of molecular motors [18]. Notably, diverse biological scenarios feature closed structures, i.e., rings or loops, as happens for DNA and RNA [19–21], extruded loops in chromatin [22,23], bacterial DNA [24–26], kinetoplast networks [27–29], and actomyosin rings [30,31]. Finally, topological constraints facilitate packing of long linear macromolecules, a process of capital importance in

eukaryotic chromosomes [32–35]. Since the dynamics of ring molecules differs dramatically from that of linear chains [32,36–41], the question about the dynamics of active rings arises naturally.

In this Letter, we characterize, by means of numerical simulations, the conformation and the dynamics of active self-avoiding polymer rings, whose monomers are self-propelled in the direction tangent to the polymer backbone; the rings are unknotted, and their topology is preserved at all times.

Our results on active self-avoiding rings show a non-monotonic dependence of the gyration radius on the ring size, in contrast with the monotonic behavior found in both passive rings and active self-avoiding linear chains, highlighting a dramatic change in their dynamics. Moreover, we identify the general pathway leading to either inflation (small rings) or collapse (large rings), along with the critical size that separates the basins of attraction of these two steady states.

Since these features are absent for active self-avoiding linear chains, clearly they are induced by the topological constraints. We prove this by comparing the dynamics of active self-avoiding rings against that of active ghost rings (that do not conserve topology). Interestingly, our results show that active ghost rings swell for all ring sizes, implying that the collapse of active rings is due to activity and collisions among non-near-neighboring monomers. Such a feature reminds that of MIPS for active Brownian particles (ABPs). Finally, focusing on collapsed rings, we find that their internal dynamics shows the hallmarks of dynamical arrest, and we observe the onset of a spinning state.

We consider fully flexible bead-spring polymer rings, suspended in an homogeneous fluid in three dimensions. We perform standard Langevin dynamics simulations neglecting hydrodynamic interactions [42]. The bead diameter σ sets the unit of length, and $m = 1$ sets the unit of mass. The active force \mathbf{f}^{act} acts with constant magnitude f^{act} along the vector tangent to the polymer backbone [13]; such construction applies to all monomers. We quantify the strength of the activity via the Péclet number $\text{Pe} \equiv f^{\text{act}}\sigma/(k_B T)$, where $k_B T$ is the thermal energy of the heat bath (k_B being the Boltzmann constant and T the absolute temperature), in which the ring polymer is suspended. Following Ref. [43], we choose to fix $f^{\text{act}}\sigma = 1$ and increase the Péclet number by decreasing the thermal energy of the heat bath. We employ a modified Kremer-Grest model to avoid crossing events and knots (Supplemental Material, Sec. 1 [44]). Hence, we simulate ring polymers of length $70 < N < 800$, at $1 < \text{Pe} < 100$; the data reported are averaged over $250 < M < 2850$ independent configurations. For tangentially active linear polymers [13,14], the average gyration radius $R_g \equiv \sqrt{\langle \sum_{i=1}^N (\mathbf{r}_i - \mathbf{r}_{\text{c.m.}})^2 / N \rangle}$ —where \mathbf{r}_i and $\mathbf{r}_{\text{c.m.}}$ are the positions of the monomer i and center of mass of the polymer, respectively—grows with N with a smaller scaling exponent, compared to the passive case, whose value depends on Pe.

In contrast, for active polymer rings, R_g shows a more complex dependence on N [Fig. 1(a)]. In particular, while for $\text{Pe} \lesssim 1$ the scaling exponent matches the equilibrium one $\nu = \nu_{\text{eq}} = 0.588$ for all values of N , for $\text{Pe} \gg 1$ two distinct regimes emerge, each of which is characterized by a specific scaling of R_g with N . For short rings $N \lesssim 100$, R_g of active rings becomes larger than R_g of passive rings. A power-law fit in this region leads to an exponent ν_{short} , that depends on Pe: At the largest activity considered ($\text{Pe} = 100$), we find $\nu_{\text{short}} \approx 1$, similar to the behavior of fully rigid rings. Hence, for short rings, the activity induces an effective bending rigidity, with a persistence length comparable to the ring size.

Upon increasing the length of the polymers [Fig. 1(a)], activity induces a structural collapse. In this regime, the scaling exponent is $\nu = \nu_{\text{long}} \approx 0.41$, and, for $\text{Pe} \geq 10$, it is independent on Pe. The small value of ν_{long} indicates that the rings assume a very compact conformation. It is worth noting that the value of ν_{long} is close to, but not exactly, the one expected in bad solvent conditions $\nu_{\text{BS}} = 0.33$ [51]. Indeed, as shown in the snapshot in Fig. 1(a), the collapsed structure is quite complex, being composed of a compact self-wrapped core and a few *dangling sections* fluttering on its surface. These dangling sections, absent in the case of ring polymers in bad solvents [52], are responsible for the larger value of ν_{long} as compared to ν_{BS} (Supplemental Material, Sec. VI [44]). Moreover, upon increasing Pe, the transition between inflated and collapsed rings becomes progressively sharper. We elucidate the role of

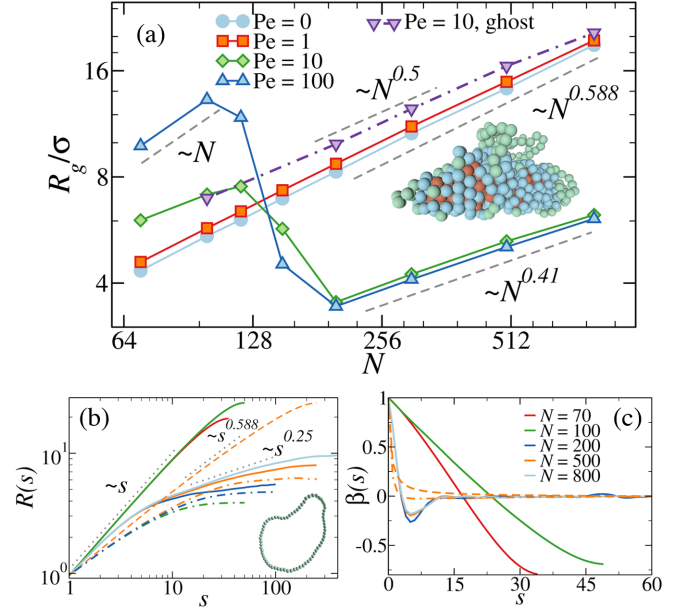


FIG. 1. (a) Gyration radius as function of N , for active self-avoiding rings (different values of Pe) and active ghost rings ($\text{Pe} = 10$) (b) Mean internal distance as function of the distance s along the contour. (c) Bond-bond correlation function as function of s . In panel (b) and (c), full lines refer to active rings at $\text{Pe} = 100$; orange dashed lines refer to the passive case in good solvent for $N = 500$; dash-dotted lines refer to the passive case in bad solvent for $N = 100, 200, 500$. Panels (b) and (c) share the legend. In panel (a) and (b) snapshots of short $N = 70$ (inflated) and long $N = 500$ (collapsed) rings, with colors referring to beads: (i) in the dangling sections or in the inflated state (green), (ii) on the surface of the collapsed structure (blue), (iii) in the interior of the collapsed core (red).

self-avoidance in this phenomenon by simulating active ghost rings that, by contrast, maintain their passive scaling $N^{0.5}$ for all values of N investigated [see the violet curve in Fig. 1(a)]; furthermore, activity swells the ghost rings, without further altering their configurational properties (Supplemental Fig. S3 [44]).

To understand the physical origin of the scaling regimes observed, we analyze the conformations attained by long and short active rings. Accordingly, we compute, in the steady state, the root mean square distance among monomers that are s th neighbors along the backbone $R(s) \equiv \sqrt{\langle (\mathbf{r}_{s+s_0} - \mathbf{r}_{s_0})^2 \rangle}$, where s_0 is the starting bead. Figure 1(b) shows that for short rings $R(s)$ displays a single power-law trend $R(s) \sim s$ whose exponent is compatible with the one estimated from the scaling of the gyration radius in Fig. 1(a). The *single* power-law fitting $R(s)$ up to $s \approx N/2$ implies the self-similarity of short active rings. For reference, we report $R_{\text{eq}}(s)$ for fully flexible passive rings in good solvents, for which $R_{\text{eq}}(s) \simeq s^{0.588}$ [52] [orange dashed lines in Fig. 1(b)]. In contrast, longer active rings show a richer behavior for $R(s)$. Indeed, for $s \lesssim 10$,

$R(s)$ displays a universal power law $R(s) \sim s$ whose prefactor does not depend on N [all curves collapse on a master curve in Fig. 1(b)]. Then, for $s \gtrsim 10$, the scaling of $R(s)$ is size dependent and, for intermediate values of s , is fitted by $R(s) \simeq s^{0.25}$. This change is the signature of the collapsed structure: Monomers very far away along the backbone end up being very close in real space. This behavior is qualitatively similar to that observed for passive rings in bad solvents [dash-dotted curves in Fig. 1(b)].

In order to characterize the local arrangement of monomers in the inflated or collapsed states, we measure the bond-bond spatial correlation function $\beta(s) \equiv \langle \mathbf{b}_{s+s_0} \cdot \mathbf{b}_{s_0} \rangle$, where $\mathbf{b}_i \equiv \mathbf{r}_{i+1} - \mathbf{r}_i$. As shown in Fig. 1(c), short active rings $N = 70$ and 100 develop a strong anticorrelation over the scale of the whole polymer, akin to rigid passive rings. In contrast, for long active rings, the bond-bond correlation function shows a very fast decay at small contour separations, followed by an anticorrelation region that eventually fades to a complete decorrelation. In the collapsed state, part of the chain wraps on itself, and such wrappings are characterized by a “pitch” of ~ 5 beads which is, roughly, at the same contour distance $s \simeq 5$ for all N and Pe investigated. Such behavior is in contrast to what is observed for passive rings in both good (dashed orange curve) and bad solvents (dotted orange curve) that display no minimum at short contour separations.

Next, we investigate the pathway from a passive, equilibrated ring configuration to the inflated or collapsed steady state, by considering the time evolution of the contour distance at which the minimum of bond correlation function appears, $\text{argmin}[\beta(s)]$, and the square average contour distance between pairs of beads that are close in space $T(t) = \langle [(j - j_1)^2 + \dots + (j - j_m)^2] / m \rangle$ that measures the “tangleness” of a polymer chain [see Supplemental Material [44], Eq. (S7)]. In particular, we follow the evolution in time of $\text{argmin}[\beta(s)]$, as it marks the characteristic size of the local structures that form along the polymer backbone [Fig. 2(a)]. For passive rings, the minimum is at $\sim N/2$ for all times. This coincides with the value obtained for active rings at early times ($t \leq 10\tau_0$); during such a time frame, comparable to the diffusion time $\tau_0 = \sigma^2/D$ of a monomer over its size, activity has not yet affected the conformation of

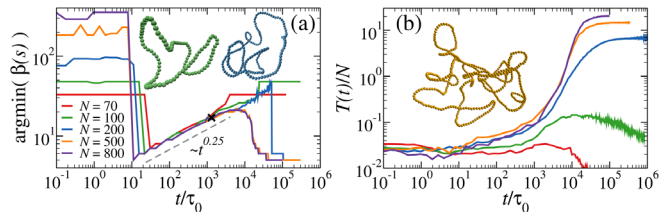


FIG. 2. Route to the steady state: (a) position of the minimum of the bond correlation; (b) tangleness $T(t)/N$ as a function of time, normalized by τ_0 , for rings of different lengths at $Pe = 100$. The black symbol in (a) marks the time at which the snapshots shown are taken. Snapshots: $N = 100$, green; $N = 200$, blue; $N = 500$, orange.

the ring. At intermediate times $t \simeq 10\tau_0 - 1000\tau_0$ (Fig. 2), small “loops” appear, highlighted by a drop of the minimum of the bond correlation to $s \simeq 5$, roughly constant for all N . Their sharp onset takes place at earlier times upon increasing the polymer size ($\sim 20\tau_0$ for $N = 70$, $\sim 10\tau_0$ for $N = 500$), and it is weakly dependent on Pe , for $Pe \gtrsim 10$. The size of the loops grows up to a characteristic amount s , reached in $t \in [\sim 10^3\tau_0; 10^4\tau_0]$, with a growth rate $\propto (t/\tau_0)^{1/4}$ essentially independent of N and Pe [for $Pe \geq 10$, Supplemental Fig. S5(b) [44]], hence setting a universal route toward the steady state. This universal growth $\propto t^{1/4}$ reminds of the coarsening of 2D ABPs undergoing MIPS [53,54]. Snapshots of rings taken during this stage are reported in Fig. 2; loops are clearly visible in all cases irrespective of N . At later times, the dynamics is no more universal, and the size of the ring matters. For $N \lesssim 100$, loops of size $s \simeq 20$ are relatively close to their equilibrium value $N/2$. When two loops meet, they merge, giving rise to a larger loop [see the jumps in $\beta(s)$ in Fig. 2(a) for $N = 70, 100$]. At variance, for $N > 200$ (Supplemental Video S1 [44]), when two loops of size $s \simeq 20$ get closer, they can thread one into the other, triggering a cascade of collisions that drives sections of the backbone to tangle, inducing the collapse of the entire chain. After such a catastrophic event, the rest of the ring is progressively recruited in the main tangle (see Supplemental Video S1 [44]). Such a scenario is also supported by the tangleness $T(t)$. Indeed, we observe the tangleness per size $T(t)/N$, at very short times, i.e., when activity has not yet affected the ring, has a characteristic value, dependent on the chosen cutoff radius r_c (defining spatial neighbors) and independent on N . Afterward, the behavior of $T(t)/N$ depends on the final steady state. For short, inflating rings, the tangleness shows a shallow maximum and then decreases. In contrast, for long collapsing rings, $T(t)/N$ monotonically increases until it reaches a large constant value. This increment develops on roughly the same timescales as the growth of $\text{argmin}[\beta(s)]$ but, furthermore, shows two regimes, characterized by a mild increase first and a steeper slope later on. These latter regimes highlight the increase of steric interactions and collisions. $T(t)$ and $\text{argmin}[\beta(s)]$ appear complementary to each other: The tangleness better captures the “two-step” collapse, while $\text{argmin}[\beta(s)]$ better highlights the universality of this route. The conformations along the pathway can be further characterized with the torsional order parameter (Supplemental Fig. S7 [44]). We remark that the collapsed state is, in its origin, akin to MIPS [6], as both are initiated by collisions and maintained by self-avoidance. This confirms the result reported for ghost rings: Without self-avoidance, tangles cannot form, and the rings are effectively composed by noninteracting loops (Supplemental Fig. S3 [44]). The described pathway is common for sufficiently high Pe , while for $Pe \approx 5$ sufficiently long rings may end up in a collapsed state following a much smoother route (Supplemental Fig. S6 [44]).

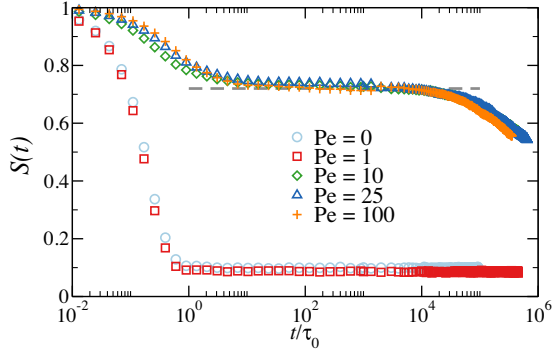


FIG. 3. Fraction of survived neighbors as function of time; data refer to rings of size $N = 500$ and several Pe at the steady state. The gray dashed line is a guide for the eye, highlighting the intermediate plateau.

After the collapse, monomers in the tangle find themselves in a complex and tight structure whose dynamics, in the steady state, is arrested. This can be verified by computing the surviving fraction of neighbors $S(t)$, defined as the fraction of the monomer’s neighbors within a radius r_c (excluding the first neighbors along the backbone), chosen at any arbitrary time t_0 during the steady state, that are still neighbors of the same monomer at $t > t_0$. We fix the neighboring cutoff $r_c = 1.2 \sigma$. Since $S(t)$ provides a measure of the permanence of the collapsed configurations, we expect $S(t) \sim 1$ for a completely frozen system; otherwise, $S(t)$ decays to a small nonvanishing value after a characteristic time. Figure 3 shows $S(t)$ for $N = 500$ and increasing activity ($Pe \in [0:100]$). For $Pe \leq 1$, rings are not collapsed and $S(t)$ displays a fast decay and plateaus to a small value, akin to passive rings [55]. As soon as the rings collapse ($Pe \geq 5$), $S(t)$ shows a strikingly different behavior. First, at short times ($t \leq \tau_0$), $S(t)$ decays mildly due to the highly mobile dangling sections. This decay occurs on a timescale comparable to that of passive rings but with reduced magnitude. The initial decay is followed by a plateau that lasts several decades and whose time span is slightly dependent on N (Supplemental Fig. S12 [44]). Afterward, a second decay is observed, which possibly plateaus at later times (outside the time frame of the simulations). This double decay can be found also in the intermediate scattering function and in the time correlation of the characteristic vectors of the ring (Supplemental Figs. S14–S17 [44]). Overall, for every observable considered, the first decay is due to the contribution of the dangling sections, whereas the second, much slower, is related to the complete rearrangement of the bead neighboring environment within a length scale of the order of σ . Another hallmark of an arrested dynamics appears also in the distribution of the instantaneous velocities of the monomers in the steady state [Fig. 4(a)]. As expected, at equilibrium ($Pe = 0$) the distribution is Maxwell-Boltzmann. Interestingly, for $Pe \lesssim 1$ the distribution is again Maxwell-Boltzmann but with an effective

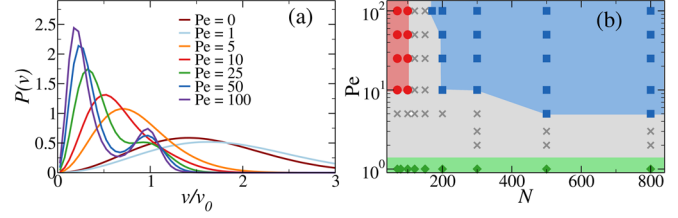


FIG. 4. (a) Monomer velocity distributions at the steady state for fixed $N = 500$, several Pe . (b) Dynamic phase diagram for active rings. Symbols refer to state points sampled by means of numerical simulations: Collapsed rings are reported as blue squares, inflated rings as red circles, passivelike rings as green diamonds, and systems showing a more complex behavior as gray crosses.

temperature $T_{\text{eff}} \simeq 1.3 k_B T^*$. At sufficiently high Pe , the distributions exhibit two peaks, at $v \ll v_0$ and $v \sim v_0$, respectively. In Fig. 4(a), the peak at small velocities is given by the monomers trapped in the collapsed section (Supplemental Fig. S18 [44]), whereas the peak at $v/v_0 \sim 1$ is due to monomers in the dangling sections. Such velocity distributions remind those observed in MIPS, where active particles inside the dense phase-separated region experience a reduced mobility with respect to their counterparts in the gas phase [56–58]. In particular, comparing Fig. 4 with Figs. 1 and 3, we note that the velocity distribution varies continuously upon increasing Pe , whereas neither the R_g nor $S(t)$ are sensitive to such a change. This implies that the configuration of the polymers, and hence the onset of a MIPS-like transition, is robust to changes in the velocity distribution provided that both Pe and N are large enough.

We collect our data into a phase diagram shown in Fig. 4(b), where four regions can be identified according to the scaling of R_g with N . At small Pe , active rings retain their equilibrium scaling for all values of N . For $Pe \gtrsim 10$, the scaling of R_g with N depends on the active ring size: Smaller active rings ($N \lesssim 100$) swell ($R_g \propto N$), whereas larger active rings ($N \gtrsim 200$) display arrested, collapsed configurations with dangling sections. The transition between these two “phases” occurs via a transition region, of finite extent, in which the dependence of R_g on N is more complex (see Fig. 1) and can be either jumping in between fairly compact and fairly open conformation (typical for $100 < N < 200$) or quasicollapsed but not arrested conformations (typical for $Pe < 5$ and $N > 300$) (Supplemental Videos S3 and S4 [44]). Finally, Supplemental Videos S1 and S2 [44] show a rotating motion and self-propulsion of the collapsed state, due to an active torque and a nonzero net active force on the center of mass, respectively [Supplemental Figs. S19 and S16(a) [44]].

In summary, we have presented the effects of tangential activity on the conformation of fully flexible self-avoiding active ring polymers. We have shown that, upon increasing the activity, there is a conformational transition between short rings ($N \lesssim 100$) that swell and assume a disklike

shape and long rings ($N \gtrsim 200$) that exhibit a structural collapse. The nonequilibrium evolution toward the steady state follows a general route featuring loop formation growing in size up to a characteristic size ~ 20 . Then, for sufficiently long rings, the collapse is triggered by clashes between monomers belonging to non-neighboring loops. Finally, the extremely slow structural relaxation of different observables indicates that the collapsed rings represent a unique example of arrested macromolecule. These features are typical of tangentially active ring polymers and may disappear in the case of isotropic [59] or scalar [60] activity. Neglecting hydrodynamics has allowed us to robustly investigate rings of large size for long timescales. Nevertheless, hydrodynamic interactions will be crucial to investigate the dynamics and the stability of the open conformations at small values of N [61]. Granted the phenomenology observed in this paper is robust, active rings may be exploited to wrap, protect, and deliver drugs. Furthermore, topology-based materials have been already proposed [62], for which activity may change the macroscopic properties, as happens for biopolymer networks [63]. Possibly, the most exciting application concerns the modeling of self-propelled filaments in gliding assays [64] and of biophysical systems, exploring the effect of activity in chromatin [65–67], in bacterial DNA and in the cytoskeleton [68–70], where the actomyosin ring may play a key role in cell division [71], or in purified protein networks [63,72,73].

The authors thank L. Tubiana for helpful discussions and acknowledge the contribution of the COST Action CA17139. V.B. acknowledges the support the European Commission through the Marie Skłodowska–Curie Fellowship No. 748170 ProFrost. The computational results presented have been achieved using the Vienna Scientific Cluster (VSC).

*emanuele.locatelli@tuwien.ac.at

Present address: Institut für Theoretische Physik, University of Vienna, Vienna 1040, Austria.

- [1] C. Bechinger, R. Di Leonardo, H. Löwen, C. Reichhardt, G. Volpe, and G. Volpe, *Rev. Mod. Phys.* **88**, 045006 (2016).
- [2] A. P. Berke, L. Turner, H. C. Berg, and E. Lauga, *Phys. Rev. Lett.* **101**, 038102 (2008).
- [3] J. Elgeti and G. Gompper, *Europhys. Lett.* **101**, 48003 (2013).
- [4] R. Di Leonardo, D. Dell’Arciprete, L. Angelani, and V. Iebba, *Phys. Rev. Lett.* **106**, 038101 (2011).
- [5] P. Magaretti, M. N. Popescu, and S. Dietrich, *Soft Matter* **14**, 1375 (2018).
- [6] M. E. Cates and J. Tailleur, *Annu. Rev. Condens. Matter Phys.* **6**, 219 (2015).
- [7] A. Kaiser, S. Babel, B. Ten Hagen, C. Von Ferber, and H. Löwen, *J. Chem. Phys.* **142**, 124905 (2015).
- [8] T. Eisenstecken, G. Gompper, and R. G. Winkler, *Polymers* **8**, 37 (2016).
- [9] R. E. Isele-Holder, J. Elgeti, and G. Gompper, *Soft Matter* **11**, 7181 (2015).
- [10] J. Yan, M. Han, J. Zhang, C. Xu, E. Luijten, and S. Granick, *Nat. Mater.* **15**, 1095 (2016).
- [11] H. R. Vutukuri, B. Bet, R. Van Roij, M. Dijkstra, and W. T. Huck, *Sci. Rep.* **7**, 16758 (2017).
- [12] S. Gonzalez and R. Soto, *New J. Phys.* **20**, 053014 (2018).
- [13] V. Bianco, E. Locatelli, and P. Magaretti, *Phys. Rev. Lett.* **121**, 217802 (2018).
- [14] S. K. Anand and S. P. Singh, *Phys. Rev. E* **98**, 042501 (2018).
- [15] M. Fogliano, E. Locatelli, C. Brackley, D. Michieletto, C. Likos, and D. Marenduzzo, *Soft Matter* **15**, 5995 (2019).
- [16] S. Das and A. Cacciuto, *Phys. Rev. Lett.* **123**, 087802 (2019).
- [17] A. Deblais, A. C. Maggs, D. Bonn, and S. Woutersen, *Phys. Rev. Lett.* **124**, 208006 (2020).
- [18] B. Alberts, A. Johnson, J. Lewis, M. Raff, K. Roberts, and P. Walter, *Molecular Biology of the Cell* (Garland Science, Oxford, 2007).
- [19] R. Schleif, *Annu. Rev. Biochem.* **61**, 199 (1992).
- [20] J.-F. Allemand, S. Cocco, N. Douarache, and G. Lia, *Eur. Phys. J. E* **19**, 293 (2006).
- [21] S. Semsey, K. Virnik, and S. Adhya, *Trends Biochem. Sci.* **30**, 334 (2005).
- [22] A. Goloborodko, J. F. Marko, and L. A. Mirny, *Biophys. J.* **110**, 2162 (2016).
- [23] W. Schwarzer, N. Abdennur, A. Goloborodko, A. Pekowska, G. Fudenberg, Y. Loe-Mie, N. A. Fonseca, W. Huber, C. H. Haering, L. Mirny *et al.*, *Nature (London)* **551**, 51 (2017).
- [24] A. Worcel and E. Burgi, *J. Mol. Biol.* **71**, 127 (1972).
- [25] L. Postow, C. D. Hardy, J. Arsuaga, and N. R. Cozzarelli, *Genes Dev.* **18**, 1766 (2004).
- [26] X. Wang, P. M. Llopis, and D. Z. Rudner, *Nat. Rev. Genet.* **14**, 191 (2013).
- [27] P. Borst and J. H. Hoeijmakers, *Plasmid* **2**, 20 (1979).
- [28] Y. Diao, V. Rodriguez, M. Klingbeil, and J. Arsuaga, *PLoS One* **10**, e0130998 (2015).
- [29] A. R. Klotz, B. W. Soh, and P. S. Doyle, *Proc. Natl. Acad. Sci. U.S.A.* **117**, 121 (2020).
- [30] I. M. Sehring, P. Recho, E. Denker, M. Kourakis, B. Mathiesen, E. Hannezo, B. Dong, and D. Jiang, *eLife* **4**, e09206 (2015).
- [31] S. P. Pearce, M. Heil, O. E. Jensen, G. W. Jones, and A. Prokop, *Bull. Math. Biol.* **80**, 3002 (2018).
- [32] A. Grosberg, Y. Rabin, S. Havlin, and A. Neer, *Europhys. Lett.* **23**, 373 (1993).
- [33] A. Rosa and R. Everaers, *PLoS Comput. Biol.* **4**, e1000153 (2008).
- [34] A. Rosa, *Biochem. Soc. Trans.* **41**, 612 (2013).
- [35] J. D. Halverson, J. Smrek, K. Kremer, and A. Y. Grosberg, *Rep. Prog. Phys.* **77**, 022601 (2014).
- [36] M. Frank-Kamenetskii, A. Lukashin, and A. Vologodskii, *Nature (London)* **258**, 398 (1975).
- [37] M. Cates and J. Deutsch, *J. Phys.* **47**, 2121 (1986).
- [38] M. Rubinstein, *Phys. Rev. Lett.* **57**, 3023 (1986).
- [39] A. Y. Grosberg, S. K. Nechaev, and E. I. Shakhnovich, *J. Phys.* **49**, 2095 (1988).

- [40] C. Micheletti, D. Marenduzzo, and E. Orlandini, *Phys. Rep.* **504**, 1 (2011).
- [41] I. Chubak, E. Locatelli, and C. N. Likos, *Mol. Phys.* **116**, 2911 (2018).
- [42] Such an approximation is made in the spirit of “dry active matter” that has identified the onset of activity-induced phase separation (known as MIPS), later observed also in experiments (hence, where hydrodynamic coupling is present). Similarly, we expect that our results will qualitatively persist even in the presence of hydrodynamic coupling.
- [43] J. Stenhammar, D. Marenduzzo, R. J. Allen, and M. E. Cates, *Soft Matter* **10**, 1489 (2014).
- [44] See Supplemental Material at <http://link.aps.org/supplemental/10.1103/PhysRevLett.126.097801> for model and simulation details, sample videos, and additional numerical data, including Refs. [45–50].
- [45] S. Plimpton, *J. Comp. Physiol.* **117**, 1 (1995).
- [46] K. Kremer and G. S. Grest, *J. Chem. Phys.* **92**, 5057 (1990).
- [47] R. Chelakkot, R. G. Winkler, and G. Gompper, *Phys. Rev. Lett.* **109**, 178101 (2012).
- [48] L. Tubiana, G. Polles, E. Orlandini, and C. Micheletti, *Eur. Phys. J. E* **41**, 72 (2018).
- [49] P.-G. de Gennes, *Scaling Concepts in Polymer Chemistry* (University Press, Ithaca, NY, 1979).
- [50] C. Kurzthaler, S. Leitmann, and T. Franosch, *Sci. Rep.* **6**, 36702 (2016).
- [51] M. Doi, *Introduction to Polymer Physics* (Clarendon Press, Oxford Science Publications, Oxford, 1996).
- [52] M. Rubinstein, R. H. Colby *et al.*, *Polymer Physics*, Vol. 23 (Oxford University Press, New York, 2003).
- [53] J. Stenhammar, A. Tiribocchi, R. J. Allen, D. Marenduzzo, and M. E. Cates, *Phys. Rev. Lett.* **111**, 145702 (2013).
- [54] A. Patch, D. Yllanes, and M. C. Marchetti, *Phys. Rev. E* **95**, 012601 (2017).
- [55] We remark that such a value is not strictly zero, as relatively close monomers can randomly get in and out of the threshold range chosen ($r_c = 1.2\sigma$).
- [56] R. Sánchez and P. Díaz-Leyva, *Physica (Amsterdam)* **499A**, 11 (2018).
- [57] S. Mandal, B. Liebchen, and H. Löwen, *Phys. Rev. Lett.* **123**, 228001 (2019).
- [58] L. Caprini and U. Marini Bettolo Marconi, [arXiv:2009.07234](https://arxiv.org/abs/2009.07234).
- [59] S. M. Mousavi, G. Gompper, and R. G. Winkler, *J. Chem. Phys.* **150**, 064913 (2019).
- [60] J. Smrek, I. Chubak, C. N. Likos, and K. Kremer, *Nat. Commun.* **11**, 26 (2020).
- [61] M. Liebetreu and C. N. Likos, *Commun. Mater.* **1**, 4 (2020).
- [62] B. A. Krajina, A. Zhu, S. C. Heilshorn, and A. J. Spakowitz, *Phys. Rev. Lett.* **121**, 148001 (2018).
- [63] G. H. Koenderink, Z. Dogic, F. Nakamura, P. M. Bendix, F. C. MacKintosh, J. H. Hartwig, T. P. Stossel, and D. A. Weitz, *Proc. Natl. Acad. Sci. U.S.A.* **106**, 15192 (2009).
- [64] L. Liu, E. Tüzel, and J. L. Ross, *J. Phys. Condens. Matter* **23**, 374104 (2011).
- [65] T. Terakawa, S. Bisht, J. M. Eeftens, C. Dekker, C. H. Haering, and E. C. Greene, *Science* **358**, 672 (2017).
- [66] D. Saintillan, M. J. Shelley, and A. Zidovska, *Proc. Natl. Acad. Sci. U.S.A.* **115**, 11442 (2018).
- [67] K. A. Haushalter and J. T. Kadonaga, *Nat. Rev. Mol. Cell Biol.* **4**, 613 (2003).
- [68] G. Danuser, J. Allard, and A. Mogilner, *Annu. Rev. Cell Dev. Biol.* **29**, 501 (2013).
- [69] M. Murrell, P. W. Oakes, M. Lenz, and M. L. Gardel, *Nat. Rev. Mol. Cell Biol.* **16**, 486 (2015).
- [70] D. A. Fletcher and R. D. Mullins, *Nature (London)* **463**, 485 (2010).
- [71] T. Litschel, C. F. Kelley, D. Holz, M. A. Koudehi, S. K. Vogel, L. Burbaum, N. Mizuno, D. Vavylonis, and P. Schwille, [bioRxiv, https://doi.org/10.1101/2020.06.30.180901](https://doi.org/10.1101/2020.06.30.180901).
- [72] S. Stam, S. L. Freedman, S. Banerjee, K. L. Weirich, A. R. Dinner, and M. L. Gardel, *Proc. Natl. Acad. Sci. U.S.A.* **114**, E10037 (2017).
- [73] F. Burla, Y. Mulla, B. E. Vos, A. Aufderhorst-Roberts, and G. H. Koenderink, *Nat. Rev. Phys.* **1**, 249 (2019).